Synthesis, Structural Analysis, and Surface Characterization of $Fe_3O_4@SiO_2$ Core–Shell Nanoparticles via Co-Precipitation

Sunil P. Gawali[a,b,*], Atul P. Keche, Ram S. Barkule[d], D.V. Mane[e,f]

[a]Department of Chemistry, Sundarrao More Arts, Commerce and Science College, Poladpur, Raigad, 402303 India
[b]School of science, Yashwantrao Chavan Maharashtra open University, Nashik, Maharashtra 402222 India
[c]Department of Physics, R B Attal Arts Science And Commerce, Georai, Beed, Maharashtra 431127 India
[d]Department of Physics, Sundarrao More Arts, Commerce and Science College, Poladpur, Raigad, 402303 India
[e]Ex. Regional Director, YCMOU Nashik 420003 India
[f]Department of Chemistry, Shri Chhatrapati Shivaji College Omerga, Dharashiv 413606 India
Corresponding Author: spgawali1986@gmail.com

Abstract

In this study, $Fe_3O_4@SiO_2$ core–shell nanoparticles were synthesized via a co-precipitation method assisted by microwave irradiation, yielding highly crystalline, well-structured nanocomposites. X-ray diffraction (XRD) analysis confirmed the formation of magnetite with an inverse spinel cubic structure, exhibiting crystallite sizes ranging from 17.9 to 28.3 nm. Structural evaluations using Williamson–Hall and Nelson–Riley analyses provided accurate estimations of lattice parameters and revealed moderate strain and defect densities. Scanning electron microscopy (SEM) and high-resolution transmission electron microscopy (HRTEM) confirmed spherical morphology with particle sizes between 69 and 196 nm, and the presence of an amorphous silica shell encapsulating a polycrystalline Fe_3O_4 core. Selected area electron diffraction (SAED) patterns supported the polycrystalline nature of the core, while energy-dispersive X-ray spectroscopy (EDS) confirmed the elemental composition with prominent signals of Fe, Si, and O. Fourier-transform infrared (FTIR) spectroscopy exhibited characteristic Si–O–Si and Fe–O stretching vibrations, validating the core–shell formation. Vibrating sample magnetometry (VSM) revealed that the nanoparticles retained superparamagnetic behavior with high saturation magnetization and low coercivity, making them magnetically responsive without remanence, thereby minimizing aggregation. The silica shell not only improved the chemical stability and biocompatibility of the particles but also provided opportunities for surface functionalization. These findings demonstrate that $Fe_3O_4@SiO_2$ nanoparticles possess excellent structural, morphological, and magnetic properties, making them highly suitable for applications in catalysis, targeted drug delivery, magnetic separation, and environmental remediation.

Keywords: Co-precipitation; $Fe3O4@SiO2$; XRD; SEM; HRTEM;

1. Introduction

The innovation of magnetite@silica ($Fe3O4@SiO2$) core shell nanoparticles lies in the strategic creation of a chemically dichotomous yet synergistically integrated system. The primary challenge with pristine magnetite nanoparticles is their inherent chemical lability; the Fe^{2+} ions are susceptible to oxidation, and the entire structure is vulnerable to degradation in acidic media, compromising its long-term magnetic and structural integrity [1]. The encapsulation by a silica (SiO_2) shell via a base-catalyzed hydrolysis and polycondensation of an alkoxysilane precursor, typically tetraethyl orthosilicate (TEOS), provides a robust chemical solution. The amorphous silica shell acts as an electronically insulating and chemically inert barrier, effectively isolating the magnetic core from oxidative and corrosive environments. More significantly, it introduces a new, highly versatile chemical interface [2]. The novelty is not merely in the passivation but in the transformation of the nanoparticle into a high-surface-area, magnetically recoverable support whose surface chemistry can be precisely engineered. The surface is densely populated with silanol (Si-OH) groups, which serve as reactive sites for covalent functionalization, allowing the nanoparticle to transition from a passive magnetic entity to an active participant in chemical transformations, most notably as a heterogeneous catalyst support [3].

The synthesis itself is a study in controlled inorganic polymerization. The synthesis of $Fe_3O_4@SiO_2$ nanoparticles is typically achieved through a multi-step process, beginning with the formation of the magnetic core of the Fe_3O_4 core via aqueous co-precipitation of Fe^{2+}/Fe^{3+} salts under alkaline conditions establishes a crystalline inverse spinel lattice, confirmed by its characteristic X-ray diffraction pattern. The subsequent Stöber method for shelling is a classic example of sol-gel chemistry, where the hydrolysis of TEOS is initiated by a base (NH_3), forming silicic acid and its oligomers. [4] These species then undergo condensation reactions ($Si-OH + HO-Si \rightarrow Si-O-Si + H_2O$) onto the surface of the dispersed $Fe3O_4$ nanoparticles, which act as nucleation seeds. The kinetics of these reactions, and thus the resulting shell thickness and porosity, are directly governed by chemical parameters such as pH, solvent polarity, and reactant concentration. Spectroscopic evidence is definitive: Fourier-Transform Infrared (FTIR) spectra display the disappearance of precursor C-H stretches and the appearance of a strong, broad asymmetric Si-O-Si stretching vibration near 1090 cm^{-1}, a hallmark of the polysiloxane network, alongside the foundational Fe-O vibration of the core around 580 cm^{-1}. This confirms the formation of a covalent inorganic polymer shell around the magnetic core [5, 6].

The true chemical elegance of $Fe3O4@SiO2$ nanoparticles is realized in their application as catalyst scaffolds, which represents a significant advancement over traditional supports. The ability to functionalize the silanol-rich surface with organosilanes, such as (*3-aminopropyl)triethoxysilane* (APTES) or (*3-mercaptopropyl*)trimethoxysilane (MPTMS), opens a gateway to covalently anchor a vast array of catalytic species. This heterogenization of homogeneous catalysts for instance, tethering palladium complexes for C-C coupling reactions (Suzuki, Heck) or rhodium complexes for hydrogenation combines the high selectivity and activity of molecular catalysts with the facile, magnetically-driven separation of a solid-phase system. A particularly novel application is the design of solid acid/base catalysts. By grafting sulfonic acid groups ($-SO_4H$) onto the silica shell, a magnetically recoverable solid acid is created, providing a recyclable and non-corrosive alternative to mineral acids for reactions like esterification and acetal formation. Conversely, immobilization of amine functionalities yields a solid base catalyst. Beyond this, the silica shell can act as a dielectric spacer in more complex photocatalytic systems, such as $Fe3O4@SiO2@TiO2$. Here, the SiO_2 layer prevents the quenching of photogenerated electron-hole pairs by the magnetic core, enhancing the photocatalytic efficiency of the outer TiO_2 layer in degrading organic pollutants. In all these catalytic applications, the superparamagnetism of the core, confirmed by Vibrating-Sample Magnetometry (VSM) showing near-zero coercivity, is critical. It ensures the catalyst remains well-dispersed during the reaction for maximum substrate interaction and then rapidly aggregates under an external magnetic field for quantitative recovery and reuse, embodying the principles of green and sustainable chemistry [7, 8].

The unique combination of magnetic responsiveness, chemical inertness, low cytotoxicity, and a highly functionalizable surface makes $Fe3O4@SiO2$ nanoparticles exceptionally valuable. Their applications are extensive and impactful, particularly in the biomedical field, where they are utilized as contrast agents for Magnetic Resonance Imaging (MRI), vehicles for targeted drug delivery, and mediators for magnetic hyperthermia cancer therapy. In biotechnology, they serve as robust, magnetically separable supports for enzyme immobilization and for the purification and separation of proteins, DNA, and cells. Furthermore, in environmental remediation, these nanoparticles are employed as efficient and recyclable adsorbents for the removal of heavy metal ions and organic pollutants from contaminated water. This broad utility underscores the importance of $Fe3O4@SiO2$ core shell nanoparticles as a powerful and adaptable platform in modern nanotechnology. The post-synthesis surface modification strategies, including silanization, polymer coating, and functionalization with biomolecules, have been explored to impart biocompatibility, targeting capabilities, and specific functionalities for diverse applications of $Fe3O4@SiO2$ core shell nanoparticles [9, 10].

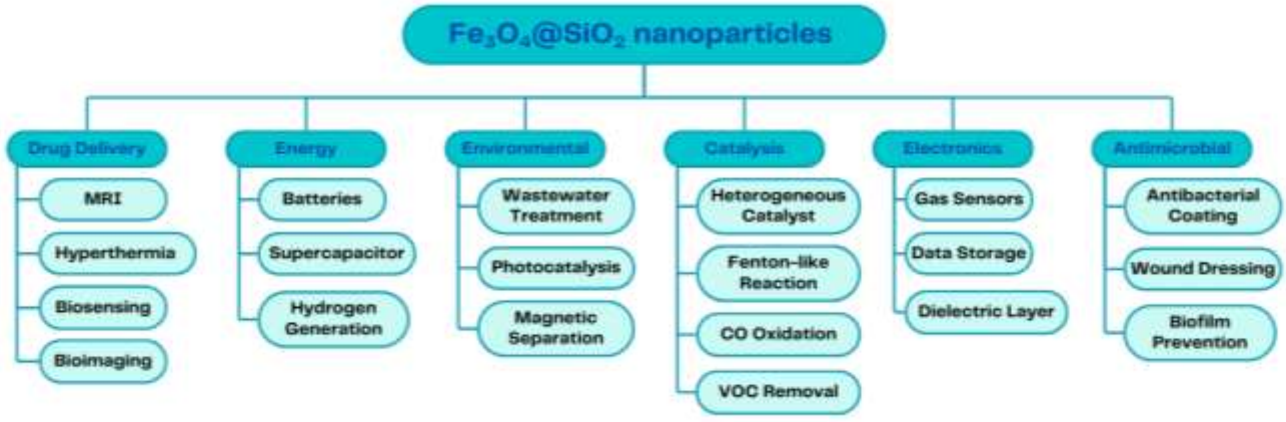

Figure 1. Various applications of $Fe_3O_4@SiO_2$ core shell nanoparticles in different areas

2. Starting materials

For the synthesis of $Fe_3O_4@SiO_2$ (magnetite@silica) core-shell nanoparticles, the starting materials include 1.0 g of Fe_3O_4 nanoparticles as the magnetic core and 200 mL of ethanol as a co-solvent. A 1:2 mixture of deionized water is used to disperse these components. To initiate silica coating, 0.1 M NaOH is added in a 3:1 ratio to adjust the pH to 11, followed by the dropwise addition of 10 mL of 30% sodium metasilicate solution as the silica precursor. 1.0 M HCl is used later to adjust the final pH to 9, facilitating the silica shell formation.

3. Preparation of $Fe_3O_4@SiO_2$ nanoparticles

The $Fe_3O_4@SiO_2$ (*magnetite@silica*) core shell nanoparticles were synthesized through a coprecipitation process assisted by a microwave treatment. Initially, 1.0 g of pre-synthesized Fe_3O_4 nanoparticles was dispersed in a 1:2 v/v mixture of deionized water and ethanol (200 mL). The solution was subjected to ultrasonication for 30 minutes to achieve a homogeneous and stable dispersion of magnetic nanoparticles. Following this, 0.1 M NaOH solution was added in a 3:1 ratio to adjust the pH to approximately 11, creating a basic environment conducive to silica deposition. Subsequently, 10 mL of 30% sodium metasilicate solution was added dropwise under continuous stirring. The basic medium facilitated the hydrolysis of sodium metasilicate, leading to the in situ formation of silanol groups (Si OH), which subsequently underwent condensation to form a uniform silica layer on the Fe_3O_4 surface. The overall hydrolysis and condensation reactions are as follows:

Hydrolysis,

$$Na_2SiO_3 + 3H_2O \rightarrow 2NaOH + H_4Si_4 \qquad (1)$$

Condensation,

$$2H_4SiO_4 \rightarrow Si - O - Si + 3H_2O_2 \qquad (2)$$

After the silica precursor was completely added, 1.0 M HCl was introduced to reduce the pH to 9, which promotes further condensation and shell formation. The reaction mixture was stirred continuously for 1 hour to ensure complete hydrolysis and uniform coating of silica onto the magnetic cores. During this process, gaseous byproducts such as CO_2 and ammonia may evolve, indicating the completion of the reaction. The resulting suspension was left undisturbed overnight (12 h) to allow proper aging of the silica network. Following this, the mixture was subjected to microwave irradiation at 700 W and 90 °C for 10 minutes, enhancing the crystallinity and shell uniformity. The product was then washed multiple times with distilled water (pH 7) and ethanol to remove unreacted reagents and byproducts. Magnetic separation using an external magnet enabled easy collection of the $Fe_3O_4@SiO_2$ nanoparticles. Finally, the collected product was dried in a hot air oven at 80 °C, yielding fine, uniformly coated $Fe_3O_4@SiO_2$ core shell nanoparticles suitable for various applications in catalysis, biomedicine, and environmental remediation. See **Figure 2** for the steps involved in the synthesis of $Fe_3O_4@SiO_2$ nanoparticles using co-precipitation.

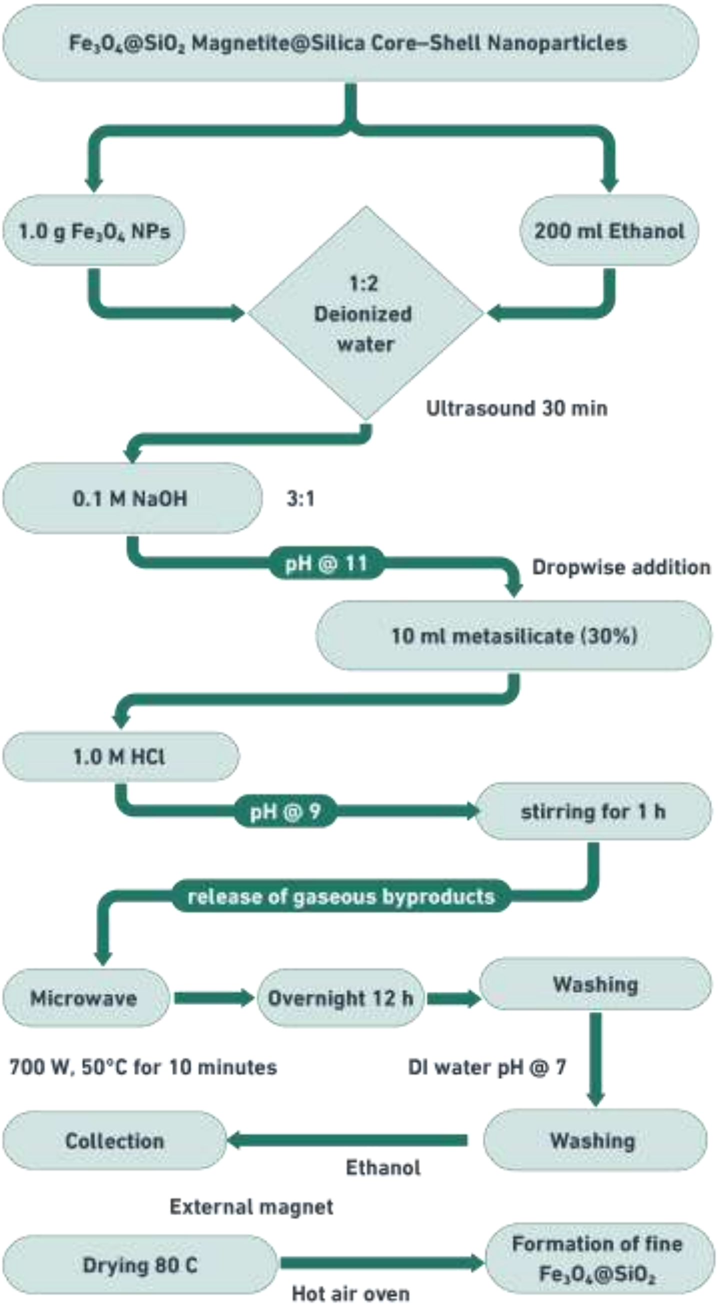

Figure 2. Co-precipitation Synthesis steps of Fe_3O_4 nanoparticles, and follow up synthesis of $Fe_3O_4@SiO_2$ nanoparticles

4. Results and discussion

4.1. XRD of $Fe_3O_4@SiO_2$ nanoparticles

The structural analysis of $Fe_3O_4@SiO_2$ nanoparticles was carried out using X-ray diffraction (XRD) with an X'pertPro MPD PANalytical system. The measurements were recorded over a 2θ range of 20° to 80°, utilizing Cu Kα radiation ($\lambda = 1.5405$ Å) at room temperature. The corresponding XRD pattern for the $Fe_3O_4@SiO_2$ nanoparticles is presented in **Figure 3**.

Detailed crystallographic parameters, including Miller indices (h, k, l), diffraction angles (2θ), half-angles (θ), trigonometric values (Sinθ and 2Sinθ), interplanar spacing (d), and lattice constants ($(a/d)^2$ and a), are summarized in **Table 1**, providing insights into the phase composition and structural characteristics of the synthesized nanoparticles.

The phase purity and crystal structure of the as-synthesized core-shell nanocomposite were elucidated by X-ray diffraction (XRD) analysis. The resulting diffractogram displays a series of five prominent and sharp reflections at 2θ angles of 30.20°, 35.55°, 43.18°, 57.25°, and 62.65°. These peaks have been indexed to the (220), (311), (400), (511), and (440) lattice planes, respectively, which are the characteristic diffraction planes of the inverse spinel cubic structure of magnetite (Fe3O4). The observed pattern aligns perfectly with the Joint Committee on Powder Diffraction Standards (JCPDS) reference card No. 19-0629, confirming the identity of the magnetic core. The pronounced sharpness of these peaks is a clear indicator of the well-defined and highly crystalline nature of the Fe3O4 core.

Further analysis involved the calculation of the lattice constant (a) from the diffraction data. The average lattice parameter was determined to be 8.366 Å. This value is in very close agreement with the standard reported value for bulk magnetite (8.396 Å), with only a minor contraction. This slight deviation from the bulk value is characteristic of nanoscale materials and is often ascribed to lattice strain and surface effects inherent in high-surface-area nanoparticles. A critical feature of the diffractogram is the conspicuous absence of any sharp peaks attributable to crystalline silica phases, such as quartz or cristobalite. This provides compelling evidence that the silica shell encapsulating the magnetic core exists in an amorphous state, which is typical for silica formed via the Stöber method. The presence of a broad, low-intensity hump, characteristic of amorphous SiO_2, is often observed between 2θ = 20-25° and would further substantiate this conclusion. In summary, the XRD results provide definitive confirmation of the successful synthesis of $Fe_3O_4@SiO_2$ nanoparticles, verifying the material consists of a highly crystalline inverse spinel magnetite core surrounded by an amorphous silica shell [11, 12].

Table 1. Miller indices of the $Fe_3O_4@SiO_2$ nanoparticles

h	**k**	**l**	**2θ**	**θ**	**Sinθ**	**2Sinθ**	**d**	**$(a/d)^2$**	**a (Å)**
2	2	0	30.200	15.100	0.261	0.521	2.956	8.036	8.361
3	1	1	35.546	17.773	0.305	0.611	2.523	11.033	8.367
4	0	0	43.177	21.589	0.368	0.736	2.093	16.030	8.372
5	1	1	57.254	28.627	0.479	0.958	1.607	27.180	8.352
4	4	0	62.649	31.325	0.520	1.040	1.481	32.004	8.380
									8.366

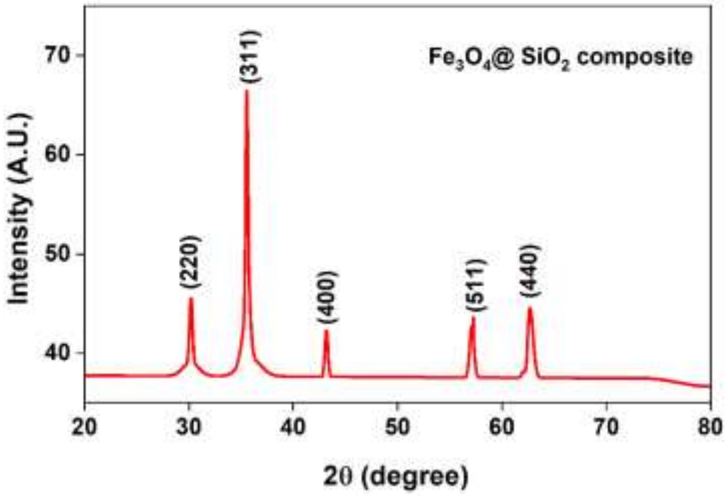

Figure 3. X-ray diffraction pattern of Fe_3O_4@SiO_2 nanoparticles

The X-ray diffraction analysis of Fe_3O_4@SiO_2 nanoparticles reveals five characteristic peaks at 2θ values ranging from 30.200° to 62.649°, with crystallite sizes varying between 17.897 nm and 28.299 nm and an average of 22.231 nm. The dislocation density exhibits an inverse correlation with crystallite size, ranging from 1.249×10^{-3} to 3.122×10^{-3} nm^{-2}, while lattice strain values span from 0.409×10^{-3} to 1.071×10^{-3}, indicating moderate structural distortion within the nanoparticles [13]. The FWHM values between 0.329° and 0.478° demonstrate reasonable peak broadening effects from finite size and strain contributions, suggesting that the silica shell successfully preserves the magnetite crystal structure despite introducing interfacial strain. The consistent crystallite size distribution and controlled dislocation densities reflect effective synthesis conditions, producing core-shell nanoparticles with maintained crystalline integrity suitable for magnetic applications requiring surface functionalization capabilities as depicted in **Table 2**.

Table 2. FWHM, Crystallite size (D), dislocation density (δ), lattice strain (ε), of the Fe_3O_4@SiO_2 nanoparticles

			FWHM					
2θ	**θ in Degree**	**Radian (θ)**	**Degree (θ)**	**Radian (θ)**	**Cos θ**	**D nm**	**δ*10^3 (nm^{-2})**	**ε*10^{-3}**
30.200	15.100	0.263	0.347	0.006	0.966	23.703	1.780	0.409
35.546	17.773	0.310	0.395	0.007	0.952	21.111	2.244	0.553
43.177	21.589	0.377	0.478	0.008	0.930	17.897	3.122	0.825

57.254	28.627	0.499	0.449	0.008	0.878	20.145	2.464	1.071
62.649	31.325	0.546	0.329	0.006	0.854	28.299	1.249	0.873
						22.231		

Table 3. lattice constant (a), bond lengths L_A, L_B, interatomic distances D_{ax}, d_{BX}, d_{AXE}, d_{BXE}, d_{BXEu}, ionic radii r_A, and r_B of the $Fe_3O_4@SiO_2$ nanoparticles

(a) Å	**L_A**	**L_B**	**d_{AX}**	**d_{BX}**	**d_{AXE}**	**d_{BXE}**	**d_{BXEu}**	**r_A**	**r_B**
8.361	2.523	2.444	1.897	2.041	3.098	2.814	2.958	0.577	0.720
8.367	2.525	2.445	1.899	2.043	3.100	2.816	2.960	0.579	0.722
8.372	2.526	2.447	1.900	2.044	3.102	2.818	2.962	0.580	0.723
8.352	2.521	2.442	1.895	2.039	3.095	2.811	2.955	0.575	0.718
8.380	2.528	2.448	1.901	2.046	3.105	2.820	2.964	0.581	0.725

Table 3 presents detailed structural parameters of the Fe_3O_4 nanoparticles, providing insight into their atomic arrangement. The structural parameters of $Fe_3O_4@SiO_2$ nanoparticles demonstrate remarkable consistency across different measurement conditions, with lattice constants ranging from 8.352 to 8.380 Å, indicating minimal structural variation within the magnetite core despite the silica coating process. The tetrahedral site bond lengths (LA) vary between 2.521 and 2.528 Å while octahedral site bond lengths (LB) span 2.442 to 2.448 Å, reflecting the characteristic spinel structure preservation with slight lattice expansion due to core-shell interactions. Interatomic distances show controlled variations, with dAX ranging from 1.895 to 1.901 Å and dBX from 2.039 to 2.046 Å, while the longer-range distances dAXE, dBXE, and dBXEu maintain proportional relationships between 2.811 and 3.105 Å. The ionic radii calculations reveal tetrahedral cation radii (rA) between 0.575 and 0.581 Å and octahedral cation radii (rB) from 0.718 to 0.725 Å, confirming the expected Fe^{3+}/Fe^{2+} distribution in the spinel lattice with minimal distortion from the silica shell formation, thereby preserving the essential magnetic properties while enabling surface functionalization capabilities [14, 15].

Table 4. θ, Sinθ, 2Sinθ, cosθ, $\cos^2\theta/\sin\theta$, F(θ), a (Å), βcosθ, and 4sinθ of the $Fe_3O_4@SiO_2$ nanoparticles determined for the Williamson-Hall plot, Bradley-Jay function, Nelson-Relay function, and Misalignment data

θ	**Sinθ**	**2Sinθ**	**cosθ**	**$\cos^2\theta$ / sinθ**	**F(θ)**	**a (Å)**	**βcosθ**	**4sinθ**
15.100	0.261	0.521	0.965	3.578	3.639	8.361	0.030	1.042
17.773	0.305	0.611	0.952	2.970	3.021	8.367	0.004	1.220
21.589	0.368	0.736	0.930	2.350	2.390	8.372	0.006	1.471

28.627	0.479	0.958	0.878	1.608	1.635	8.352	0.001	1.916
31.325	0.520	1.040	0.854	1.403	1.427	8.380	0.011	2.079

Williamson-Hall analysis

The Williamson-Hall analysis data for Fe_3O_4@SiO_2 nanoparticles presents comprehensive trigonometric functions and structural parameters across five diffraction angles from 15.100° to 31.325°, where the systematic progression of $\sin\theta$ values from 0.261 to 0.520 and corresponding $\cos\theta$ values from 0.965 to 0.854 enables accurate strain-size separation through linear plotting techniques. The $\cos^2\theta/\sin\theta$ ratios decrease progressively from 3.578 to 1.403, while the $F(\theta)$ function values follow a similar trend from 3.639 to 1.427, providing essential correction factors for precise lattice parameter determination across different crystallographic orientations. The calculated lattice constants exhibit minimal variation between 8.352 and 8.380 Å, confirming structural uniformity despite the core-shell configuration, while the $\beta\cos\theta$ values range from 0.001 to 0.030, indicating low instrumental broadening contributions to the overall peak width. The $4\sin\theta$ parameters spanning 1.042 to 2.079 facilitate the construction of modified Williamson-Hall plots that effectively separate crystallite size and microstrain effects, demonstrating that the silica coating process maintains the magnetite lattice integrity while introducing controllable structural modifications suitable for advanced magnetic nanoparticle applications (**Figure 4**)[16, 17].

Nelson-Riley Function

The **Figure 5** demonstrates Nelson-Riley function plot demonstrates a systematic linear relationship between the lattice parameter 'a' and the extrapolation function $F(\theta) = (cos^2\theta/sin\theta + cos^2\theta/\theta)/2$ for Fe_3O_4@SiO_2 nanoparticles, with data points exhibiting excellent linearity across the angular range. The intercept value of 8.37189 ± 0.01623 Å represents the most accurate lattice parameter determination, effectively minimizing systematic errors inherent in XRD measurements through angular extrapolation techniques. The negative slope of -0.00223 ± 0.00634 indicates minimal angular-dependent systematic errors, confirming the reliability of the structural analysis. This extrapolation method proves particularly valuable for core-shell nanoparticles where precise lattice parameter determination is crucial for understanding the structural integrity of the magnetite core despite silica coating effects. The tight clustering of experimental points around the linear fit validates the consistency of the crystallographic measurements and demonstrates that the Nelson-Riley approach successfully eliminates angular-dependent measurement uncertainties.

Bradley-Jay Function

The Bradley-Jay function plot reveals a strong negative correlation between $\text{Cos}\theta$ and $2\text{Sin}\theta$ parameters, with the linear fit yielding an intercept of 1.08267 ± 0.0093 and a slope of -0.21571 ± 0.01166, demonstrating excellent experimental precision in the structural characterization as shown in **Figure 6**. This analytical approach effectively separates instrumental broadening from sample-related peak broadening effects, providing insights into the crystallite size and strain contributions within the $Fe_3O_4@SiO_2$ nanoparticles. As per the formula $a = \lambda/(2sin\theta) \cdot \sqrt{(h^2 + k^2 + l^2)}$, the systematic decrease in Cosθ values from approximately 0.97 to 0.85 as 2Sinθ increases from 0.5 to 1.1 follows the expected trigonometric relationship while maintaining minimal scatter around the fitted line. The high linearity observed in this plot confirms the absence of significant preferred orientation effects and validates the assumption of isotropic crystallite size distribution within the core-shell structure. This function proves essential for accurate microstructural parameter extraction in nanoparticle systems where conventional analysis methods may introduce systematic errors [18, 19].

Misalignment

The misalignment function plot in **Figure 7** exhibits a pronounced linear decrease in $Cos^2\theta/Sin\theta$ values from approximately 3.6 to 1.4 as the diffraction angle θ increases from 15° to 31°, with exceptional linearity characterized by an intercept of 5.34915 ± 0.30354 and slope of -0.12968 ± 0.0128. With the $\Delta(2\theta) = s \cdot cos^2\theta/sin\theta$, the systematic angular dependence reflects the geometric correction necessary for accurate structural parameter determination in powder diffraction analysis of $Fe_3O_4@SiO_2$ nanoparticles. The excellent fit quality demonstrates minimal instrumental misalignment effects during data collection, confirming proper experimental setup and sample preparation procedures. The negative slope indicates successful correction for angular-dependent systematic errors that commonly arise in nanoparticle diffraction studies, particularly important for core-shell materials where accurate structural characterization is essential for property optimization. This misalignment correction function ensures that the extracted lattice parameters and microstructural information accurately represent the true crystallographic properties of the magnetite core within the silica-coated nanoparticles [20].

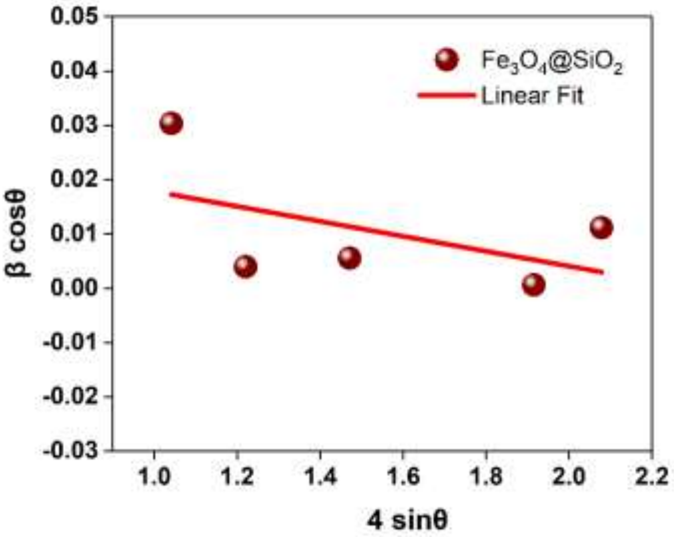

Figure 4. Williamson-Hall extrapolation of $Fe_3O_4@SiO_2$ nanoparticles

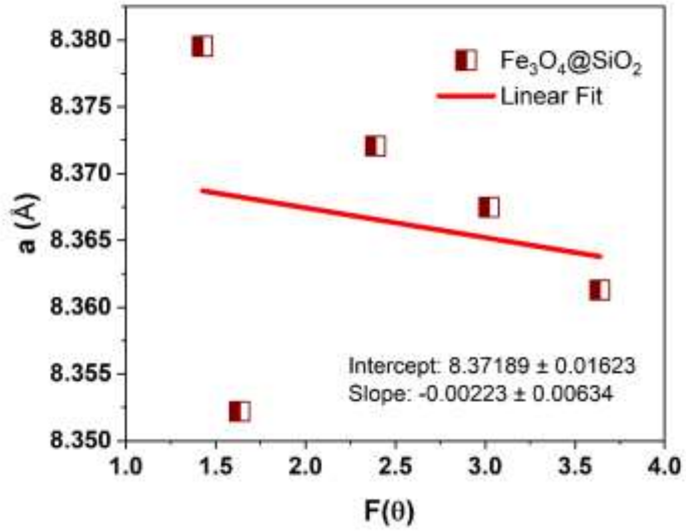

Figure 5. Nelson Relay Function of $Fe_3O_4@SiO_2$ nanoparticles

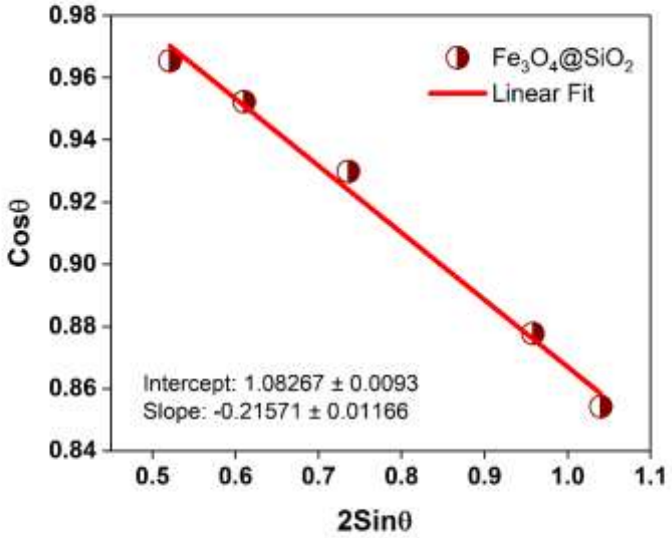

Figure 6. Bradly-Jay Function of $Fe_3O_4@SiO_2$ nanoparticles

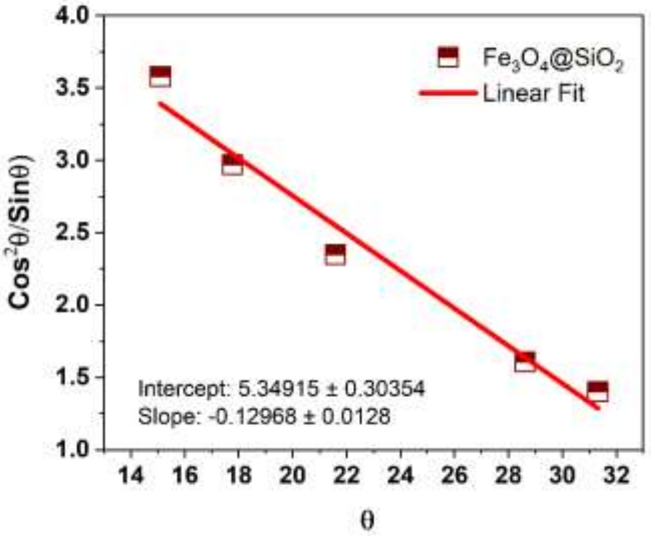

Figure 7. Misalignment of $Fe_3O_4@SiO_2$ nanoparticles

4.2. Microstructure of $Fe_3O_4@SiO_2$ nanoparticles

Scanning Electron Microscopy (SEM) analysis was conducted using a Field Emission Gun-Scanning Electron Microscope (FEG-SEM), Model JSM-7600F, at the Sophisticated Analytical Instrument Facility (SAIF), IIT Bombay, Mumbai. The SEM micrographs of $Fe_3O_4@SiO_2$ nanoparticles with a composition ratio of $x = 0.6$, as presented in **Figure 8 (a-d)**, provide detailed insights into the surface morphology at a magnification of 500,000×, with a scale bar of 300 nm. The images indicate that the nanoparticles exhibit a predominantly spherical shape, with particle sizes ranging between 69 and 196 nm. Although minor agglomeration is evident an expected feature in nanomaterials the particles demonstrate a well-defined core-shell architecture, essential for enhanced stability and suitability across various functional applications [21].

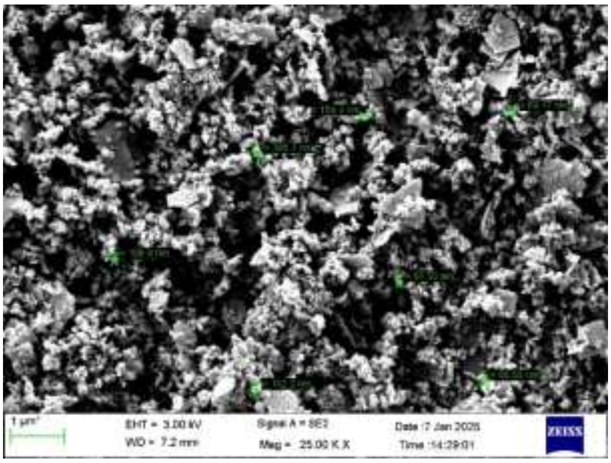
1 µm
EHT = 3.00 kV
WD = 7.2 mm
Signal A = SE2
Mag = 25.00 K X
Date :7 Jan 2025
Time :14:29:01
ZEISS

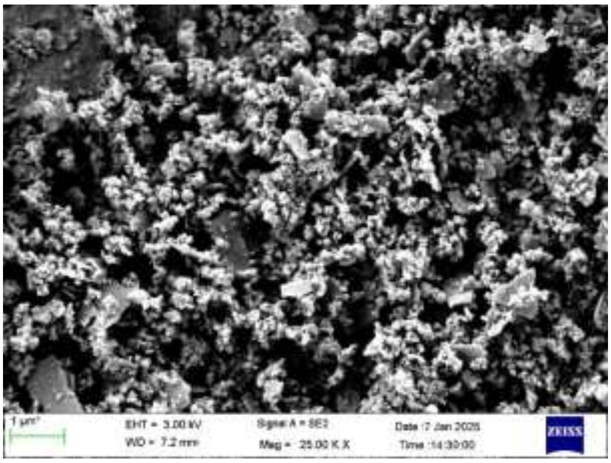
1 µm
EHT = 3.00 kV
WD = 7.2 mm
Signal A = SE2
Mag = 25.00 K X
Date :7 Jan 2025
Time :14:30:00
ZEISS

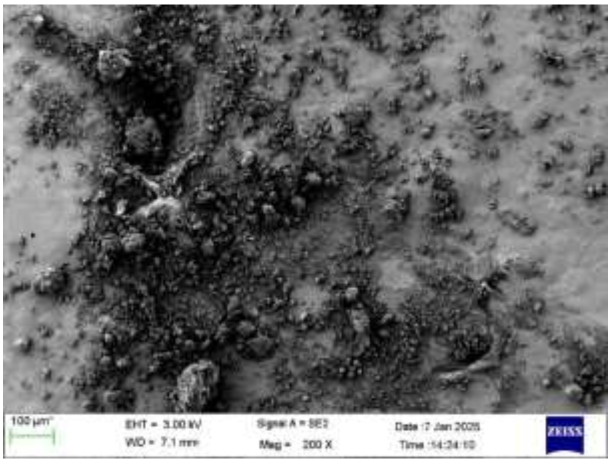
100 µm
EHT = 3.00 kV
WD = 7.1 mm
Signal A = SE2
Mag = 200 X
Date :7 Jan 2025
Time :14:24:10
ZEISS

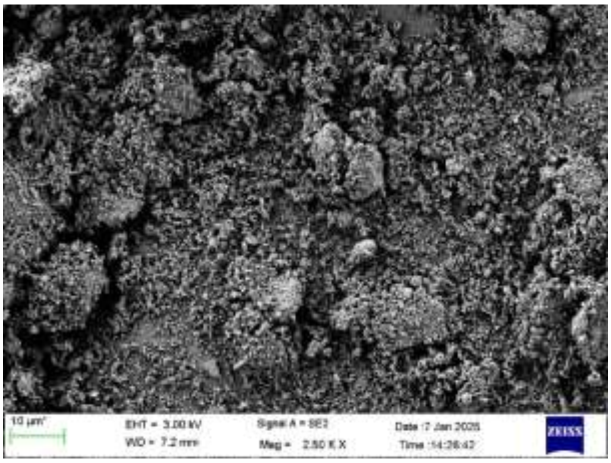
10 µm
EHT = 3.00 kV
WD = 7.2 mm
Signal A = SE2
Mag = 2.50 K X
Date :7 Jan 2025
Time :14:26:42
ZEISS

Figure 8 (a-d). SEM image of $Fe_3O_4@SiO_2$ nanoparticles

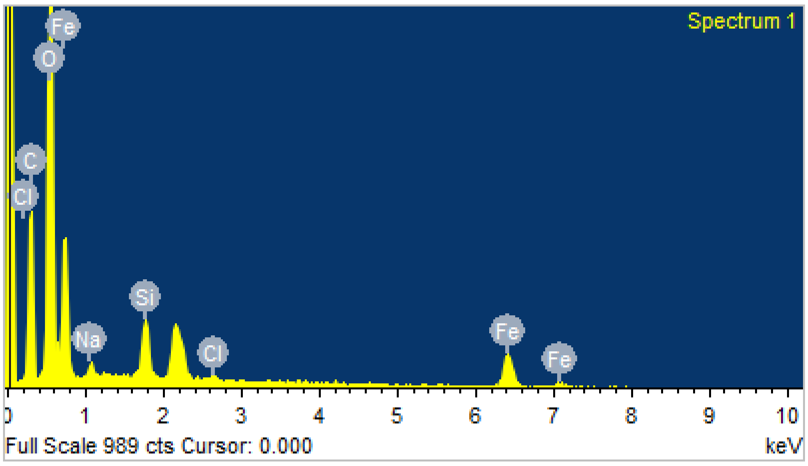

Figure 9. EDAX image of $Fe_3O_4@SiO_2$ nanoparticles

Figure 9 displays the energy-dispersive X-ray spectroscopy (EDAX) spectrum of the $Fe_3O_4@SiO_2$ nanoparticles. The EDS spectrum of the $Fe_3O_4@SiO_2$ nanoparticles confirms the successful synthesis of the core-shell structure, showing prominent peaks for Iron (Fe), Oxygen (O), and Silicon (Si). Minor peaks for Carbon (C), Sodium (Na), and Chlorine (Cl) are also present, likely due to synthesis residues or environmental contamination. Overall, the elemental analysis validates the intended $Fe_3O_4@SiO_2$ composition [22, 23].

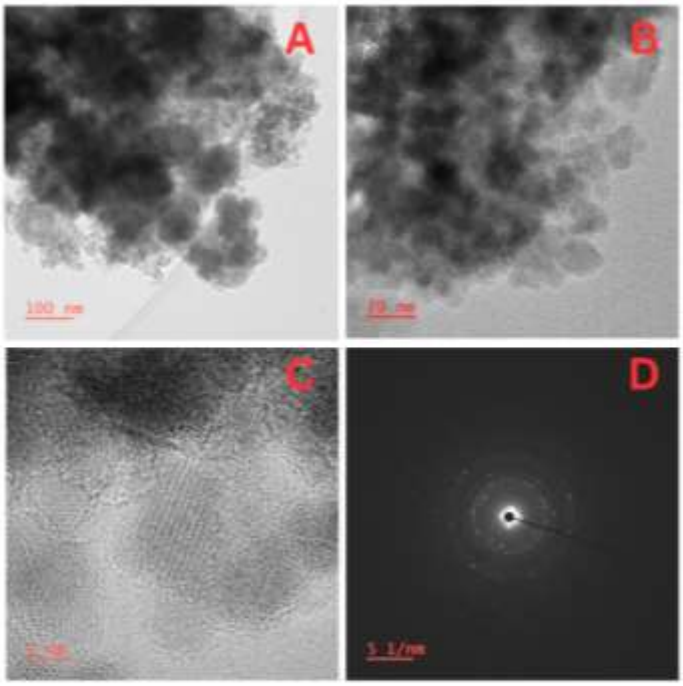

Figure 10 (a-c) HRTEM **(d)** SAED image of $Fe_3O_4@SiO_2$ nanoparticles

The high-resolution transmission electron microscopy (HRTEM) images (A-D) offer comprehensive information regarding the morphology and structural characteristics of $Fe_3O_4@SiO_2$ nanoparticles as shown in **Figure 10 (a-c)**. Images A and B, captured at varying magnifications, distinctly exhibit the core-shell configuration, where the dense Fe_3O_4 core appears darker and is encased within a lighter, amorphous silica (SiO_2) shell. The nanoparticles maintain a mostly spherical geometry with noticeable agglomeration, aligning with the features observed in SEM analysis. In Image C, the lattice fringes of the Fe_3O_4 core are clearly visible, confirming its crystalline phase, whereas the surrounding silica lacks defined fringes, indicative of its amorphous structure. The selected area electron diffraction (SAED) pattern shown in Image **Figure 10(d)** presents concentric diffraction rings, characteristic of a polycrystalline Fe_3O_4 core embedded within an amorphous matrix, affirming the successful synthesis of the core-shell architecture [24, 25].

4.3 FTIR spectra of $Fe_3O_4@SiO_2$ nanoparticles

The FTIR spectrum demonstrates successful encapsulation of Fe_3O_4 nanoparticles with a silica layer. The Si-O-Si stretching peak around 1022 cm^{-1} and Fe-O bands near 533 and 461 cm^{-1} provide clear evidence of the core shell structure as shown in **Figure 11**. Additionally, the O-H and H-O-H bands point to the hydrophilic nature of the surface, likely due to silanol (Si-OH) groups, which can enhance dispersion in aqueous media and offer sites for further surface functionalization. The spectrum confirms the structural integrity of both components magnetite and silica while also suggesting some surface hydration and minor residuals from synthesis [26, 27].

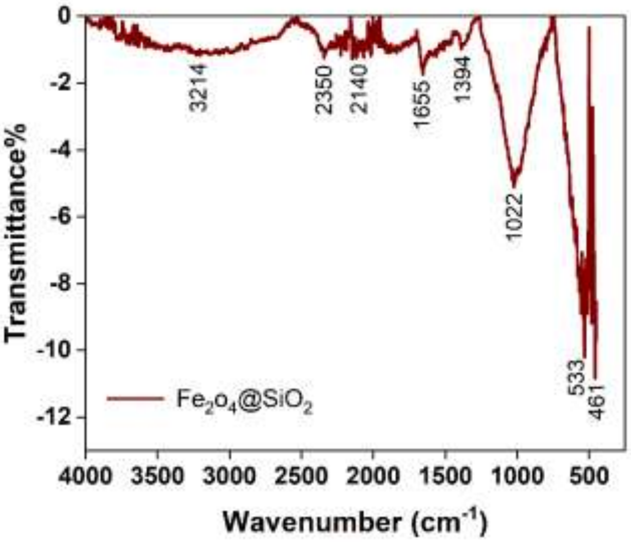

Figure 11 FTIR spectra of $Fe_3O_4@SiO_2$ nanoparticles

4.4 VSM of $Fe_3O_4@SiO_2$ nanoparticles

The VSM results affirm that the $Fe_3O_4@SiO_2$ nanoparticles retain strong magnetic properties, despite being coated with a silica shell as shown in **Figure 12**. The observed superparamagnetic behavior ensures that the nanoparticles do not retain magnetization once the external magnetic field is removed, preventing particle agglomeration and making them suitable for biomedical and catalytic applications. The high saturation magnetization combined with low coercivity highlights the efficiency of the magnetic core, while the silica coating offers additional benefits such as improved biocompatibility, chemical stability, and functionalization capability. The magnetic profile confirms the successful formation of core-shell Fe_3O_4@SiO_2 nanostructures with promising potential for multifunctional applications [28, 29].

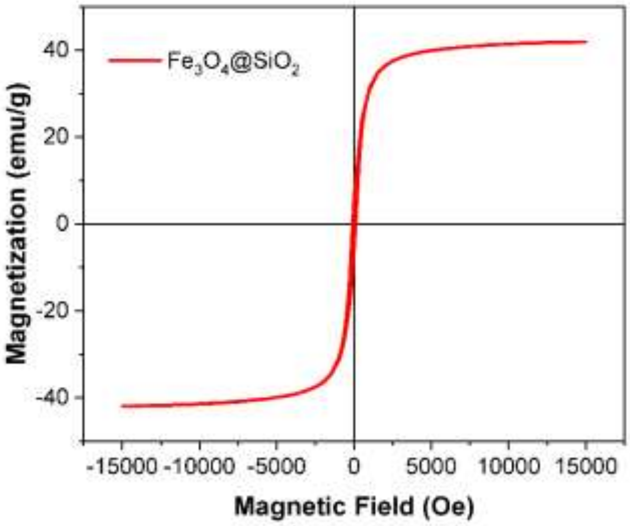

Figure 12 Hysteresis loop of Fe_3O_4@SiO_2 nanoparticles

5. Conclusion

The Fe_3O_4@SiO_2 core–shell nanoparticles were successfully synthesized via a co-precipitation method assisted by microwave irradiation, resulting in highly crystalline and structurally well-defined nanocomposites. X-ray diffraction (XRD) analysis confirmed the formation of magnetite with an inverse spinel cubic structure, and the silica coating did not disrupt the core phase. Crystallite sizes ranged from 17.9 to 28.3 nm, with an average of 22.2 nm, while structural strain and dislocation density values indicated moderate distortion and defect density. Advanced analysis using Williamson–Hall, Nelson–Riley, and other trigonometric functions provided refined estimates of lattice parameters and confirmed the crystallographic accuracy of the synthesized material. SEM and HRTEM images revealed a nearly spherical morphology with particle sizes between 69–196 nm and an amorphous silica shell surrounding a polycrystalline magnetite core, validated by SAED patterns. Elemental composition from EDS spectra confirmed the presence of Fe, O, and Si, supporting the successful formation of the core–shell structure, with minor residuals attributed to synthesis byproducts. FTIR spectroscopy further validated the core–shell architecture with distinct Si–O–Si and Fe–O vibrational bands. VSM measurements demonstrated superparamagnetic behavior with high saturation magnetization and low coercivity, indicating the retention of magnetic properties after silica encapsulation. This combination of strong magnetism and inert silica coating not only prevents agglomeration but also enhances chemical stability and functional versatility. The synthesized Fe_3O_4@SiO_2 nanoparticles exhibit excellent structural integrity, magnetic responsiveness, and surface functionality, making them highly suitable for a wide range of applications such as catalysis, drug delivery, magnetic separation, and environmental remediation.

Reference

[1] A.-L. Morel, S.I. Nikitenko, K. Gionnet, A. Wattiaux, J. Lai-Kee-Him, C. Labrugere, B. Chevalier, G. Deleris, C. Petibois, A. Brisson, Sonochemical approach to the synthesis of Fe3O4@ SiO2 core− shell nanoparticles with tunable properties, ACS nano, 2 (2008) 847-856.
[2] M. Sonmez, M. Georgescu, L. Alexandrescu, D. Gurau, A. Ficai, D. Ficai, E. Andronescu, Synthesis and applications of Fe3O4/SiO2 core-shell materials, Current pharmaceutical design, 21 (2015) 5324-5335.
[3] H. Ding, Y. Zhang, S. Wang, J. Xu, S. Xu, G. Li, Fe3O4@ SiO2 core/shell nanoparticles: the silica coating regulations with a single core for different core sizes and shell thicknesses, Chemistry of Materials, 24 (2012) 4572-4580.
[4] G.S. An, J.S. Han, J.R. Shin, D.H. Chae, J.U. Hur, H.-Y. Park, Y.-G. Jung, S.-C. Choi, In situ synthesis of Fe3O4@ SiO2 core–shell nanoparticles via surface treatment, Ceramics International, 44 (2018) 12233-12237.
[5] D. Salman, T. Juzsakova, M. Al-Mayyahi, R. Ákos, S. Mohsen, R. Ibrahim, H.D. Mohammed, T. Abdullah, E. Domokos, T. Korim, Synthesis, surface modification and characterization of magnetic Fe3O4@ SiO2 core-shell nanoparticles, Journal of Physics: Conference Series, IOP Publishing, 2021, pp. 012039.
[6] A. Khalid, R. Ahmed, M. Taha, T. Soliman, Fe3O4 nanoparticles and Fe3O4@ SiO2 core-shell: synthesize, structural, morphological, linear, and nonlinear optical properties, Journal of Alloys and Compounds, 947 (2023) 169639.
[7] M. Gao, W. Li, J. Dong, Z. Zhang, B. Yang, Synthesis and characterization of superparamagnetic Fe3O4@ SiO2 core-shell composite nanoparticles, World Journal of Condensed Matter Physics, 1 (2011) 49-54.
[8] R. Roto, Y. Yusran, A. Kuncaka, Magnetic adsorbent of Fe3O4@ SiO2 core-shell nanoparticles modified with thiol group for chloroauric ion adsorption, Applied Surface Science, 377 (2016) 30-36.
[9] O. Veiseh, J.W. Gunn, M. Zhang, Design and fabrication of magnetic nanoparticles for targeted drug delivery and imaging, Advanced drug delivery reviews, 62 (2010) 284-304.
[10] S.S. Alterary, A. AlKhamees, Synthesis, surface modification, and characterization of Fe3O4@ SiO2 core@ shell nanostructure, Green Processing and Synthesis, 10 (2021) 384-391.
[11] F. Babaei, A. Ghasemi, Structural, optical and magnetic properties of nickel–copper ferrite NixCu1− x Fe 2O4, Optical and Quantum Electronics, 54 (2022) 697.
[12] S.A.J. Mohammed, B.K. Al-Rawi, R.M. Al-Haddad, Fe3O4@ SiO2 core–shell nanoparticles: Synthesis, characterization prepared by green method for iraqi aloe vera extract, International Journal of Nanoscience, 22 (2023) 2350009.
[13] R.M. Cornell, U. Schwertmann, The iron oxides: structure, properties, reactions, occurrences, and uses, Wiley-vch Weinheim2003.
[14] E. Verwey, E. Heilmann, Physical properties and cation arrangement of oxides with spinel structures I. Cation arrangement in spinels, The Journal of Chemical Physics, 15 (1947) 174-

180.

[15] M.E. Fleet, The structure of magnetite, Structural Science, 37 (1981) 917-920.

[16] G. Williamson, W. Hall, X-ray line broadening from filed aluminium and wolfram, Acta metallurgica, 1 (1953) 22-31.

[17] V. Mote, Y. Purushotham, B. Dole, Williamson-Hall analysis in estimation of lattice strain in nanometer-sized ZnO particles, Journal of theoretical and applied physics, 6 (2012) 1-8.

[18] A.J.C. Wilson, Mathematical theory of X-ray powder diffractometry, (No Title), DOI (1963).

[19] A. Taylor, H. Sinclair, On the determination of lattice parameters by the Debye-Scherrer method, Proceedings of the Physical Society, 57 (1945) 126.

[20] J.I. Langford, A rapid method for analysing the breadths of diffraction and spectral lines using the Voigt function, Applied Crystallography, 11 (1978) 10-14.

[21] H. Mahajan, S.K. Godara, A. Srivastava, Synthesis and investigation of structural, morphological, and magnetic properties of the manganese doped cobalt-zinc spinel ferrite, Journal of Alloys and Compounds, 896 (2022) 162966.

[22] J.I. Goldstein, D.E. Newbury, J.R. Michael, N.W. Ritchie, J.H.J. Scott, D.C. Joy, Scanning electron microscopy and X-ray microanalysis, springer2017.

[23] R.F. Egerton, Physical principles of electron microscopy, Springer2005.

[24] G.F. Goya, T. Berquo, F.C. Fonseca, M. Morales, Static and dynamic magnetic properties of spherical magnetite nanoparticles, Journal of applied physics, 94 (2003) 3520-3528.

[25] T. Daou, G. Pourroy, S. Bégin-Colin, J.-M. Greneche, C. Ulhaq-Bouillet, P. Legaré, P. Bernhardt, C. Leuvrey, G. Rogez, Hydrothermal synthesis of monodisperse magnetite nanoparticles, Chemistry of materials, 18 (2006) 4399-4404.

[26] A. Andrade, D. Souza, M. Pereira, J. Fabris, R. Domingues, Synthesis and characterization of magnetic nanoparticles coated with silica through a sol-gel approach, Cerâmica, 55 (2009) 420-424.

[27] H. Namduri, S. Nasrazadani, Quantitative analysis of iron oxides using Fourier transform infrared spectrophotometry, Corrosion Science, 50 (2008) 2493-2497.

[28] A.G. Roca, L. Gutiérrez, H. Gavilán, M.E.F. Brollo, S. Veintemillas-Verdaguer, M. del Puerto Morales, Design strategies for shape-controlled magnetic iron oxide nanoparticles, Advanced drug delivery reviews, 138 (2019) 68-104.

[29] M. Mahmoudi, S. Sant, B. Wang, S. Laurent, T. Sen, Superparamagnetic iron oxide nanoparticles (SPIONs): development, surface modification and applications in chemotherapy, Advanced drug delivery reviews, 63 (2011) 24-46.